Supplementary Information

Phosphorescent Organometallic Knots of Gold(I)-Bis(acetylide) Strands Directed by Copper(I) π-Coordination

Ya-Zi Huang,[1,3] Jin-Yun Wang,[1] Zhu Jiao,[1] Pei Xie,[1] Zhong-Ning Chen[1,2] ✉

[1] State Key Laboratory of Structural Chemistry Fujian Institute of Research on the Structure of Matter, Chinese Academy of Sciences 155, Yangqiao Road West, Fuzhou, Fujian 350002, China

[2] Fujian Science and Technology Innovation Laboratory for Optoelectronic Information of China, Fuzhou, Fujian 350108, China

[3] University of Chinese Academy of Sciences, Beijing, 100039, China

E-mail: czn@fjirsm.ac.cn

EXPERIMENTAL SECTION

Physical Measurements. UV-Vis absorption spectra were measured on a Perkin-Elmer Lambda 365 UV-Vis spectrophotometer. Infrared spectra (IR) were recorded on a Bruker VERTEX 70 FT-IR spectrophotometer with KBr pellets. High resolution mass spectrometry (HRMS) was recorded on a Bruker Impact II Q-TOF mass spectrometer using dichloromethane and methanol mixtures as mobile phases. ^{1}H and ^{31}P NMR spectra were performed on a Bruker Avance III 400 spectrometer with $SiMe_4$ and H_3PO_4 as internal and external references, respectively. Emission and excitation spectra and emission lifetimes in degassed solutions, solid states and films were determined on an Edinburgh analytical instrument (FLS 920 fluorescence spectrometer). Absolute quantum yields were determined by the integrating sphere (142 mm in diameter) using Edinburgh FLS920 Spectrofuorophotometer. Cyclic voltammetry was performed with a CH Instruments Model CHI620E (CH Instruments, Inc.).

Crystal Structural Determination. Crystals suitable for X-ray crystallographic measurement were grown by layering Et_2O or *n*-hexane onto corresponding solutions or directly crystallized from reaction solutions. The X-ray single-crystal diffraction data were collected on a Bruker D8 Venture diffractometer using IμS 3.0 microfocus source Mo-Kα radiation (λ = 0.71073 Å) and PHOTON II CPAD detector. Frames were integrated with the Bruker SAINT software package (V8.38A) using a SAINT algorithm. Data were corrected for absorption effects using the multi-scan method (SADABS).[1] The structures were solved and refined using the Bruker SHELXTL Software Package, a computer program for automatic solution of crystal structures, and refined by the full-matrix least-squares method with ShelXle Version 4.8.6, a Qt graphical user interface for the SHELXL.[2] All non-hydrogen atoms were refined anisotropically, whereas the hydrogen atoms were generated geometrically and refined using isotropic thermal parameters. Eight $HNEt_3^+$ counterions in unit cells of complexes **1**, **3** and **4** and four ones in complex **2** that are too disordered to be located. The severely disordered $HNEt_3^+$ together with other disordered solvents were squeezed out using SQUEEZE/PLATON procedure.

Computational Method. The calculations were implemented by using Gaussian 16 program package[3] for complexes **1–4**. The geometrical structures as isolated molecules in the ground state and the lowest-energy triplet state were firstly optimized, respectively, by the restricted and unrestricted density functional theory (DFT) method with the gradient corrected correlation functional PBE1PBE.[4] The initial structures of complexes **1–4** were extracted from the crystal structural data. To save computational time, the reduced models were used, in which the *tert*-butyl in HL^-/L^{2-} were replaced by H atoms except for complex **2**. To analyze the absorption and emission transition properties, 80 singlet and 6 triplet excited-states were calculated, respectively, based on the optimized structures in

the ground state and lowest-energy triplet state to determine the vertical excitation energies by time-dependent density functional theory (TD-DFT)[5-7] with the same functional used in the optimization process. In the calculation of structural optimization and excited states, the Solvation Model Based on Density (SMD)[8] with CH_2Cl_2 as solvent was employed. The self-consistent field (SCF) convergence criterions of RMS density matrix and maximum density matrix were set by default in the excited-state calculation. The iterations of excited states continue until the changes on energies of states were no more than 10^{-7} a.u. between the iterations, and then convergences reached in all the excited states. In these calculations, the Stuttgart-Dresden (SDD)[9] basis set and the effective core potentials (ECPs) were used to describe the Au and Cu atoms, while other non-metal atoms of P, N, C and H were described by the all-electron basis set of 6-31G**. Visualization of the frontier molecular orbitals were performed by GaussView. The contributions of fragments to the orbitals in the electronic excitation process were analyzed by the Ros & Schuit method[10] (C-squared population analysis method, SCPA) in Multiwfn 3.7 program.[11]

Table S1. Crystallographic Data of Au-Cu Cluster Complexes **1–4**.

	1	**2**	**3**	**4**
empirical formula	$C_{204}H_{220}Au_6Cu_4N_{10}$	$C_{260}H_{272}Au_{10}Cu_4N_{10}P_4$	$C_{168}H_{202}Au_6Cu_2N_{10}$	$C_{204}H_{216}Au_8Cu_6N_{10}$
formula weight	4247.85	5884.56	3670.26	4764.83
crystal system	monoclinic	triclinic	monoclinic	monoclinic
space group	*C*2/*c*	$P\bar{1}$	*C*2/*c*	*C*2/*c*
a (Å)	42.304(4)	18.240(4)	34.044(3)	22.9670(12)
b (Å)	12.4954(12)	25.481(5)	19.6078(18)	28.1979(16)
c (Å)	39.273(3)	31.410(5)	40.167(3)	39.221(2)
α (deg)		89.152(6)		
β (deg)	102.817(2)	83.396(6)	105.596(3)	92.129(2)
γ (deg)		78.725(6)		
V (Å^3)	20243(3)	14221(4)	25825(4)	25383(2)
Z	4	2	4	4
F (000)	8416	5736.0	7248.0	9264
ρ_{calcd} (g/cm^3)	1.394	1.374	0.944	1.247
μ (mm^{-1})	4.790	5.495	3.587	5.134
Radiation (λ, Å)	0.71073	0.71073	0.71073	0.71073
temperature (K)	150(2)	120	150(2)	100(2)
GOF	1.068	1.039	1.059	1.018
R1 (F_o)[a]	0.0992	0.0664	0.0932	0.0584
*w*R2 (F_o^2)[b]	0.2735	0.2072	0.2675	0.1694

[a] $R1 = \Sigma|F_o - F_c|/\Sigma F_o$, [b] $wR2 = \Sigma[w(F_o^2 - F_c^2)^2]/\Sigma[w(F_o)^2)]^{1/2}$

Table S2. Selective interatomic distances (Å) and bonding angles (°) of Au_6Cu_4 Cluster Complex **1**.

interatomic distance			
Au1-Au1a	3.0883(14)	Au1-Cu1	2.990(2)
Au1-Cu2	2.975(3)	Au2-Cu1	2.874(3)
Au2-Cu2	2.809(3)	Au3-Cu1	2.760(4)
Au3-Cu2	2.921(2)	Au1-C1	2.02(2)
Au1-C25	1.958(17)	Au2-C48	2.019(17)
Au2-C73	1.99(2)	Au3-C24	2.04(2)
Au3-C49	1.99(3)	Cu1-C24	2.15(3)
Cu1-C25	2.09(2)	Cu1-C73	2.06(2)
Cu2-C1	2.091(18)	Cu2-C48	2.20(2)
Cu2-C49	2.027(19)		
bond angle			
Au2-Cu1-Au1	73.08(6)	Au3-Cu1-Au2	73.76(7)
Au3-Cu1-Au2	73.76(7)	Au2-Cu2-Au1	74.24(7)
Au3-Cu2-Au1	72.04(6)	Au2-Cu2-Au3	72.32(6)
C25-Au1-C1	174.7(8)	C73-Au2-C48	175.4(8)
C49-Au3-C24	176.5(10)	C73-Cu1-C24	120.3(8)
C73-Cu1-C25	124.9(9)	C25-Cu1-C24	112.6(7)
C1-Cu2-C48	111.1(9)	C49-Cu2-C1	124.3(9)
C49-Cu2-C48	122.1(7)		

Table S3. Selective interatomic distances (Å) and bonding angles (°) of $Au_{10}Cu_4$ Cluster Complex **2**.

interatomic distance			
Au1-Cu1	2.8419(16)	Au2-Au6	3.0937(8)
Au1-Cu2	2.9232(15)	Au3-C136	1.990(12)
Au1-Au10	3.1504(9)	Au3-C64	2.009(10)
Au1-Au2	3.3445(8)	Au3-Cu2	2.8175(14)
Au2-C88	1.983(10)	Au3-Cu1	2.8988(16)
Au2-C40	2.002(11)	Au3-Au9	3.1716(9)
Au2-Cu2	2.9695(16)	Au4-C73	1.974(11)
Au2-Cu1	2.9728(16)	Au4-C160	1.989(12)
Au4-Cu4	2.8328(14)	Au6-C1	1.964(10)
Au4-Cu3	2.8708(15)	Au6-C49	1.998(9)
Au4-Au7	3.0377(9)	Au6-Cu4	2.9761(15)
Au5-C25	1.992(11)	Au6-Cu3	2.9993(16)
Au5-C184	2.008(10)	Au7-C169	2.017(13)
Au5-Cu3	2.8325(15)	Au9-C97	1.984(16)
Au5-Cu4	2.8686(14)	Au8-C145	1.995(14)
Au5-Au8	3.3417(9)	Au10-C121	2.007(17)
bond angle			
Cu1-Au1-Cu2	93.67(4)	Cu1-Au2-Au6	134.85(4)
Cu1-Au1-Au10	126.51(4)	Cu2-Au2-Au1	54.77(3)
Cu2-Au1-Au10	132.90(3)	Cu1-Au2-Au1	53.07(3)
Cu1-Au1-Au2	56.75(3)	Au6-Au2-Au1	150.89(2)
Cu2-Au1-Au2	56.08(3)	Cu2-Au3-Au9	122.17(3)
Au10-Au1-Au2	123.00(2)	Cu1-Au3-Au9	134.72(4)
Cu2-Au2-Cu1	90.09(4)	Cu4-Au4-Cu3	94.36(4)
Cu2-Au2-Au6	134.72(3)	Cu4-Au4-Au7	123.10(3)
Cu3-Au4-Au7	134.36(3)	Au1-Cu1-Au3	77.66(4)
Cu3-Au5-Au8	114.64(3)	Au1-Cu1-Au2	70.18(3)

Cu4-Au5-Au8	140.91(3)	Au3-Cu1-Au2	71.07(3)
Au4-Cu3-Au6	72.34(3)	Au3-Cu2-Au1	77.64(4)
Cu4-Au6-Cu3	88.88(4)	Au3-Cu2-Au2	72.23(3)
Cu4-Au6-Au2	134.49(3)	Au1-Cu2-Au2	69.16(3)
Cu3-Au6-Au2	136.04(3)	Au5-Cu3-Au4	76.32(4)
Au5-Cu3-Au6	70.93(3)		

Table S4. Selective interatomic distances (Å) and bonding angles (°) of Au_6Cu_2 Cluster Complex **3**.

interatomic distance			
Au1-C50	2.002(11)	Au2-Au4	3.1490(12)
Au1-Cu1	2.8534(15)	Au1-Au3	3.1804(8)
Au1-Cu1a	2.8710(16)	Au4-Cu1	2.8653(16)
Au2-C1	1.966(15)	Cu1-C49	2.487(14)
Au1-C26	2.007(12)	Cu1-C70	2.075(13)
Au3-C27	1.887(17)	Cu1-C50	2.126(14)
Au3-C51	2.055(14)	Cu1-C26	2.148(16)
Au4-C70	2.013(13)	Cu1-C69	2.413(14)
Au4-C70	2.8653(16)	Cu1-C25	2.419(14)
bond angle			
Au-Cu1-Au4	78.01(4)	C70-Cu1-C26	120.7(5)
Cu1-Au1-Cu1	87.13(5)	C50-Cu1-C26	118.7(5)
Cu-Au1-Au3	135.92(4)	C70-Cu1-C69	28.5(5)
Cu1-Au1-Au3a	136.86(3)	C50-Cu1-C69	109.5(5)
Cu1-Au4-Cu1	87.02(6)	C26-Cu1-C69	125.0(5)
Cu1-Au4-Au2	136.49(3)	C70-Cu1-C25	106.7(5)
Au1-Cu1-Au1	77.54(4)	C26-Cu1-C25	30.2(5)
Au4-Cu1-Au1	77.73(4)	C69-Cu1-C25	99.2(5)
C50-Au1-C26	178.8(6)	C70-Cu1-C49	126.4(5)
C1-Au2-C1	179.0(12)	C50-Cu1-C49	29.4(4)
C70-Au4-C70	177.1(7)	C26-Cu1-C49	106.0(5)
C70-Cu1-C50	120.6(5)	C69-Cu1-C49	103.0(4)

Table S5. Selective interatomic distances (Å) and bonding angles (°) of Au_8Cu_6 Cluster Complex **4**.

interatomic distance			
Au1-Au1a	3.3109(8)	Au1-Au2	3.3793(6)
Au2-Au4	3.2907(7)	Au1-Cu1	2.8675(12)
Au1-Cu2	2.8910(13)	Au1a-Cu1	2.9516(12)
Au2-Cu2	2.6439(14)	Au3-Cu1	2.7253(13)
Au3-Cu1a	2.7255(13)	Au4-Cu3	2.8145(18)
Au1-C1	2.009(9)	Au1-C25	1.993(9)
Au2-C24	1.934(10)	Au2-C72	2.031(11)
Au3-C49	2.025(10)	Au3-C49a	2.025(10)
Au4-C48	1.969(17)	Au4-C96	2.000(15)
Au5-C73	2.017(16)	Au5-C73a	2.017(16)
Cu1-C1	2.200(10)	Cu1-C25	2.130(11)
Cu1-C49	2.077(11)	Cu2-C1	2.205(10)
Cu2-C72	2.124(12)	Cu2-C73	2.082(13)
Cu3-C24	2.138(12)	Cu3-C48	2.159(17)
bond angle			
Au1-Cu1-Au1	69.34(3)	Au3-Cu1-Au1	76.60(3)
Au3-Cu1a-Au1	78.04(3)	C72-Cu2-C1	99.6(4)
C73-Cu2-C72	152.6(5)	C73-Cu2-C1	107.7(5)
C25-Au1-C1	178.8(4)	C24-Au2-C72	174.9(5)
C49-Au3-C49	175.9(6)	C48-Au4-C96	178.0(7)
C73-Au5-C73	171.0(8)	C25-Cu1-C1	105.0(4)
C49-Cu1-C25	137.8(4)	C49-Cu1-C1	116.2(4)
C72-Cu2-C1	99.6(4)	C73-Cu2-C1	107.7(5)
C73-Cu2-C72	152.6(5)	C24-Cu3-C48	109.8(5)

Table S6. The Partial Molecular Orbital Compositions (%) by SCPA Approach and the Absorption Transitions in the Ground State for Au_6Cu_4 Complex **1** in CH_2Cl_2 Solution, Calculated by TD-DFT Method at the PBE1PBE Level.

orbital	energy (eV)	MO contribution (%)			
		Cu (s/p/d)	Au (s/p/d)	L^{2-}	HL^-
L+8	-0.72	16.78 (62/33/5)	15.32 (51/42/7)	45.36	22.54
L+7	-0.78	5.85 (4/78/18)	15.19 (10/85/6)	47.55	31.41
L+6	-0.78	11.07 (83/14/3)	54.11 (43/56/1)	10.59	24.23
L+4	-0.83	33.65 (69/30/1)	11.18 (12/79/9)	39.94	15.22
L+1	-1.07	32.11 (86/14/1)	33.32 (30/63/7)	13.42	21.15
LUMO	-1.32	31.20 (85/14/1)	26.11 (27/65/9)	23.58	19.11
HOMO	-4.73	19.97 (5/2/93)	10.39 (30/9/62)	62.08	7.56
H-1	-4.83	25.41 (1/2/97)	10.05 (44/14/42)	50.39	14.15
H-3	-5.07	29.23 (0/3/97)	7.72 (10/7/83)	35.99	27.07
H-5	-5.20	30.85 (29/5/66)	11.52 (13/30/56)	26.57	31.07
H-6	-5.23	19.68 (20/6/74)	18.70 (38/14/48)	58.50	3.13
H-7	-5.23	16.76 (3/2/95)	60.93 (57/6/37)	18.73	3.58
H-11	-5.50	35.08 (3/2/95)	18.59 (13/25/62)	34.35	11.98

state	*E*, nm (eV)	O.S.	transition (contrib.)	assignment	measured (nm)
S_1	454 (2.73)	0.0222	HOMO→LUMO (91%)	^{1}LMCT/^{1}MC/^{1}IL/^{1}LLCT	
S_6	391 (3.17)	0.4396	H-7→LUMO (53%)	^{1}MC/^{1}MLCT/^{1}IL	395
			H-5→LUMO (16%)	^{1}MC/^{1}IL/^{1}LMCT	
S_{16}	372 (3.33)	0.3682	H-3→L+1 (29%)	^{1}MC/^{1}IL/^{1}LMCT	375
			HOMO→L+8 (20%)	^{1}IL/^{1}MC/^{1}LLCT	
S_{19}	364 (3.40)	0.5175	HOMO→L+7 (49%)	^{1}IL/^{1}MC/^{1}MLCT/^{1}LLCT	
			H-6→LUMO (10%)	^{1}MC/^{1}IL/^{1}LMCT/^{1}LLCT	

Table S7. The Partial Molecular Orbital Compositions (%) by SCPA Approach and the Emission Transitions in the Lowest-Energy Triplet State for Au_6Cu_4 Complex **1** in CH_2Cl_2 Solution, Calculated by TD-DFT Method at the PBE1PBE Level.

orbital	energy (eV)	MO contribution (%)			
		Cu (s/p/d)	Au (s/p/d)	L^{2-}	HL^-
L+1	-1.22	27.99 (84/14/2)	25.60 (18/74/8)	15.02	31.39
LUMO	-1.37	27.31 (87/12/2)	24.14 (33/61/7)	14.76	33.79
HOMO	-4.68	22.71 (2/4/94)	10.04 (28/16/56)	48.31	18.94
H-2	-4.96	28.20 (4/4/92)	10.42 (31/12/57)	31.64	29.75

state	*E*, nm (eV)	O.S.	transition (contrib.)	assignment	measured (nm)
T_1	578 (2.14)	0.0000	HOMO→LUMO (32%)	^{3}MC/^{3}LMCT/^{3}IL/^{3}LLCT	530
			HOMO→L+1 (12%)	^{3}MC/^{3}LMCT/^{3}IL/^{3}LLCT	
			H-2→LUMO (12%)	^{3}MC/^{3}IL/^{3}LLCT/^{3}LMCT	

Table S8. The Partial Molecular Orbital Compositions (%) by SCPA Approach and the Absorption Transitions in the Ground State for $Au_{10}Cu_4$ Complex **2** in CH_2Cl_2 Solution, Calculated by TD-DFT Method at the PBE1PBE Level.

orbital	energy (eV)	MO contribution (%)			
		Cu (s/p/d)	Au (s/p/d)	L^{2-}	dppb
L+6	-0.80	9.96 (18/76/6)	36.25 (54/43/3)	47.66	6.13
L+5	-0.82	11.64 (55/39/6)	21.04 (6/88/6)	63.18	4.13
L+4	-0.86	24.57 (37/60/3)	23.00 (28/67/5)	49.83	2.60
L+3	-0.88	24.56 (54/43/3)	17.16 (36/54/11)	56.69	1.60
L+2	-0.93	18.97 (59/38/3)	30.36 (21/75/4)	48.81	1.86
L+1	-0.98	19.10 (72/26/2)	46.03 (52/43/6)	32.05	2.83
LUMO	-1.25	21.58 (69/28/2)	30.91 (13/79/8)	44.94	2.58
HOMO	-4.78	17.18 (5/3/92)	16.08 (35/20/45)	66.31	0.43
H-1	-4.85	22.00 (8/3/89)	15.61 (32/32/36)	62.04	0.35
H-2	-4.99	19.45 (12/5/83)	9.40 (17/13/71)	70.67	0.48
H-3	-5.06	16.34 (10/6/83)	26.67 (53/17/30)	56.42	0.57
H-5	-5.09	19.73 (29/7/64)	14.25 (31/42/27)	65.55	0.48
H-7	-5.22	21.01 (13/8/79)	20.11 (45/25/30)	58.51	0.37

state	*E*, nm (eV)	O.S.	transition (contrib.)	assignment	measured (nm)
S_1	438 (2.83)	0.0031	HOMO→LUMO (91%)	^{1}IL/^{1}MC/^{1}LMCT	432
S_5	397 (3.12)	0.3488	H-3→LUMO (68%)	^{1}IL/^{1}MC/^{1}LMCT	
S_8	385 (3.22)	0.2494	H-7→LUMO (28%)	^{1}IL/^{1}MC/^{1}LMCT	382
			HOMO→L+2 (16%)	^{1}IL/^{1}MC/^{1}LMCT	
			H-1→L+1 (11%)	^{1}MC/^{1}IL/^{1}LMCT	
S_{10}	379 (3.27)	0.1789	HOMO→L+3 (64%)	^{1}IL/^{1}MC	
			H-1→L+4 (14%)	^{1}IL/^{1}MC/^{1}LMCT	
S_{18}	363 (3.42)	0.4759	HOMO→L+5 (16%)	^{1}IL/^{1}MC	
			H-2→L+2 (14%)	^{1}IL/^{1}MC/^{1}LMCT	
			H-1→L+5 (11%)	^{1}IL/^{1}MC	
S_{23}	358 (3.46)	0.3164	H-1→L+6 (15%)	^{1}IL/^{1}MC/^{1}LMCT	
			H-2→L+4 (11%)	^{1}IL/^{1}MC/^{1}LMCT	

Table S9. The Partial Molecular Orbital Compositions (%) by SCPA Approach and the Emission Transitions in the Lowest-Energy Triplet State for $Au_{10}Cu_4$ Complex **2** in CH_2Cl_2 Solution, Calculated by TD-DFT Method at the PBE1PBE Level.

orbital	energy (eV)	MO contribution (%)			
		Cu (s/p/d)	Au (s/p/d)	L^{2-}	dppb
L+1	-1.14	21.06 (63/33/4)	30.48 (41/51/8)	45.70	2.76
LUMO	-1.28	24.60 (80/18/2)	30.54 (28/64/8)	41.78	3.09
HOMO	-4.70	21.08 (12/4/84)	17.96 (28/35/37)	60.52	0.44

state	*E*, nm (eV)	O.S.	transition (contrib.)	assignment	measured (nm)
T_1	570 (2.17)	0.0000	HOMO→LUMO (28%)	^{3}MC/^{3}IL/^{3}LMCT	545
			HOMO→L+1 (26%)	^{3}IL/^{3}MC/^{3}LMCT	

Table S10. The Partial Molecular Orbital Compositions (%) by SCPA Approach and the Absorption Transitions in the Ground State for Au_6Cu_2 Complex **3** in CH_2Cl_2 Solution, Calculated by TD-DFT Method at the PBE1PBE Level.

orbital	energy (eV)	MO contribution (%)		
		Cu (s/p/d)	Au (s/p/d)	L^{2-}
L+5	-0.30	3.90 (8/72/19)	16.29 (59/33/8)	79.82
L+4	-0.31	4.05 (10/70/21)	14.80 (52/40/8)	81.15
L+3	-0.38	7.76 (24/67/8)	13.97 (41/52/6)	78.27
L+2	-0.38	7.60 (5/86/9)	14.54 (37/57/6)	77.85
L+1	-0.41	29.18 (94/6/1)	7.97 (6/84/11)	62.85
LUMO	-0.69	33.82 (94/6/0)	23.84 (46/45/10)	42.34
HOMO	-4.38	17.13 (0/6/94)	12.29 (23/6/71)	70.57
H-1	-4.39	16.87 (0/7/92)	12.24 (21/6/73)	70.89
H-2	-4.55	18.80 (10/4/86)	12.64 (36/18/45)	68.56
H-3	-4.57	14.21 (49/3/47)	16.87 (26/24/50)	68.92
H-4	-4.57	23.93 (0/4/95)	7.46 (37/17/46)	68.61
H-5	-4.77	21.09 (11/2/87)	28.52 (45/3/52)	50.40
H-6	-4.77	21.05 (0/2/98)	31.79 (47/2/52)	47.16
H-7	-4.79	19.39 (59/2/39)	9.22 (8/35/58)	71.40

state	*E*, nm (eV)	O.S.	transition (contrib.)	assignment	measured (nm)
S_1	417 (2.98)	0.0037	HOMO→LUMO (77%)	^{1}LMCT/^{1}MC/^{1}IL	
S_2	415 (2.99)	0.0153	H-1→LUMO (77%)	^{1}LMCT/^{1}MC/^{1}IL	
S_3	397 (3.12)	0.0977	H-2→LUMO (42%)	^{1}LMCT/^{1}MC/^{1}IL	
			H-4→LUMO (24%)	^{1}MC/^{1}LMCT/^{1}IL	
S_4	396 (3.13)	0.1017	H-4→LUMO (54%)	^{1}MC/^{1}LMCT/^{1}IL	381
			H-2→LUMO (16%)	^{1}LMCT/^{1}MC/^{1}IL	
S_{10}	363 (3.42)	0.5276	H-7→LUMO (19%)	^{1}MC/^{1}LMCT/^{1}IL	
			H-5→LUMO (12%)	^{1}MC/^{1}IL/^{1}LMCT	
S_{11}	362 (3.42)	0.3735	H-1→L+3 (21%)	^{1}IL/^{1}MC	
			H-6→LUMO (16%)	^{1}MC/^{1}IL	
S_{12}	362 (3.42)	0.3010	H-1→L+4 (21%)	^{1}IL/^{1}MC	
			HOMO→L+5 (20%)	^{1}IL/^{1}MC/^{1}MLCT	
S_{13}	360 (3.44)	0.4102	H-1→L+5 (20%)	^{1}LLCT/^{1}IL/^{1}MC	
			HOMO→L+2 (18%)	^{1}IL/^{1}MC	

Table S11. The Partial Molecular Orbital Compositions (%) by SCPA Approach and the Emission Transitions in the Lowest-Energy Triplet State for Au_6Cu_2 Complex **3** in CH_2Cl_2 Solution, Calculated by TD-DFT Method at the PBE1PBE Level.

orbital	energy (eV)	MO contribution (%)		
		Cu (s/p/d)	Au (s/p/d)	L^{2-}
LUMO	-0.81	26.15 (92/6/2)	20.22 (58/32/9)	53.63
HOMO	-4.20	23.93 (3/4/93)	13.09 (32/10/58)	62.98

state	*E*, nm (eV)	O.S.	transition (contrib.)	assignment	measured (nm)
T_1	585 (2.12)	0.0000	HOMO→LUMO (63%)	^{3}MC/^{3}IL/^{3}LMCT	550

Table S12. The Partial Molecular Orbital Compositions (%) by SCPA Approach and the Absorption Transitions in the Ground State for Au_8Cu_6 Complex **4** in CH_2Cl_2 Solution, Calculated by TD-DFT Method at the PBE1PBE Level.

orbital	energy (eV)	MO contribution (%)		
		Cu (s/p/d)	Au (s/p/d)	L^{2-}
L+6	-0.86	23.47 (68/26/6)	37.63 (46/50/4)	38.90
L+4	-1.01	14.10 (53/41/6)	28.37 (50/47/3)	57.53
L+3	-1.10	20.09 (66/29/5)	26.43 (45/50/4)	53.48
L+2	-1.12	32.60 (61/37/2)	17.62 (34/60/6)	49.78
LUMO	-1.54	23.49 (78/20/2)	39.78 (40/55/5)	36.73
HOMO	-4.89	20.81 (4/8/88)	10.24 (9/24/66)	68.96
H-1	-4.95	27.65 (12/7/81)	15.68 (35/32/32)	56.67
H-3	-5.12	19.95 (33/8/58)	21.37 (34/40/26)	58.68
H-5	-5.18	24.78 (17/6/77)	10.47 (21/26/53)	64.75
H-6	-5.31	16.68 (33/12/56)	15.69 (21/34/46)	67.63
H-8	-5.41	25.20 (6/4/90)	36.89 (50/3/47)	37.91

state	*E*, nm (eV)	O.S.	transition (contrib.)	assignment	measured (nm)
S_1	465 (2.67)	0.0498	HOMO→LUMO (84%)	^{1}LMCT/^{1}MC/^{1}IL	
S_5	413 (3.00)	0.1054	H-5→LUMO (50%)	^{1}MC/^{1}LMCT/^{1}IL	
			H-3→LUMO (26%)	^{1}MC/^{1}LMCT	
S_9	393 (3.15)	0.2188	H-8→LUMO (44%)	^{1}MC/^{1}IL	391
			H-6→LUMO (22%)	^{1}LMCT/^{1}MC	
			H-3→LUMO (11%)	^{1}MC/^{1}LMCT	
S_{16}	379 (3.28)	0.3899	H-1→L+2 (47%)	^{1}MC/^{1}IL/^{1}LLCT	
			HOMO→L+3 (19%)	^{1}MC/^{1}LLCT/^{1}LMCT	
S_{26}	363 (3.42)	0.4431	HOMO→L+4 (21%)	^{1}LLCT/^{1}MC/^{1}LMCT	
			HOMO→L+6 (20%)	^{1}LMCT/^{1}MC/^{1}IL	

Table S13. The Partial Molecular Orbital Compositions (%) by SCPA Approach and the Emission Transitions in the Lowest-Energy Triplet State for Au_8Cu_6 Complex **4** in CH_2Cl_2 Solution, Calculated by TD-DFT Method at the PBE1PBE Level.

orbital	energy (eV)	MO contribution (%)		
		Cu (s/p/d)	Au (s/p/d)	L^{2-}
L+1	-1.22	28.69 (70/27/3)	31.93 (35/59/6)	39.38
LUMO	-1.68	27.24 (77/21/2)	32.65 (41/52/7)	40.11
HOMO	-4.75	26.53 (5/9/87)	12.14 (23/25/52)	61.33

state	*E*, nm (eV)	O.S.	transition (contrib.)	assignment	measured (nm)
T_1	592 (2.09)	0.0000	HOMO→LUMO (63%)	^{3}MC/^{3}LMCT/^{3}IL	600
			HOMO→L+1 (10%)	^{3}MC/^{3}LMCT/^{3}IL	

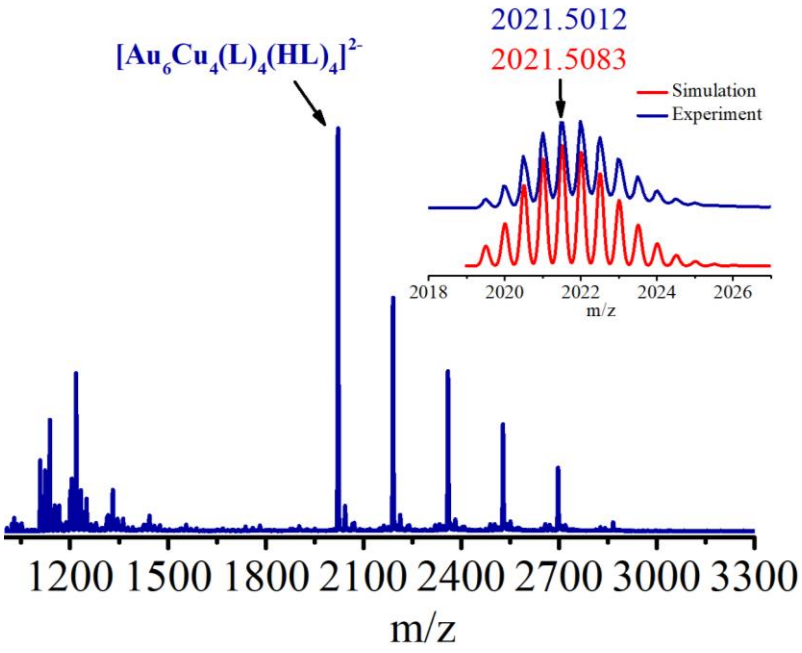

Figure S1. The high-resolution mass spectrometry of Au_6Cu_4 complex **1**. Inset: the measured (blue) and simulated (red) isotopic patterns.

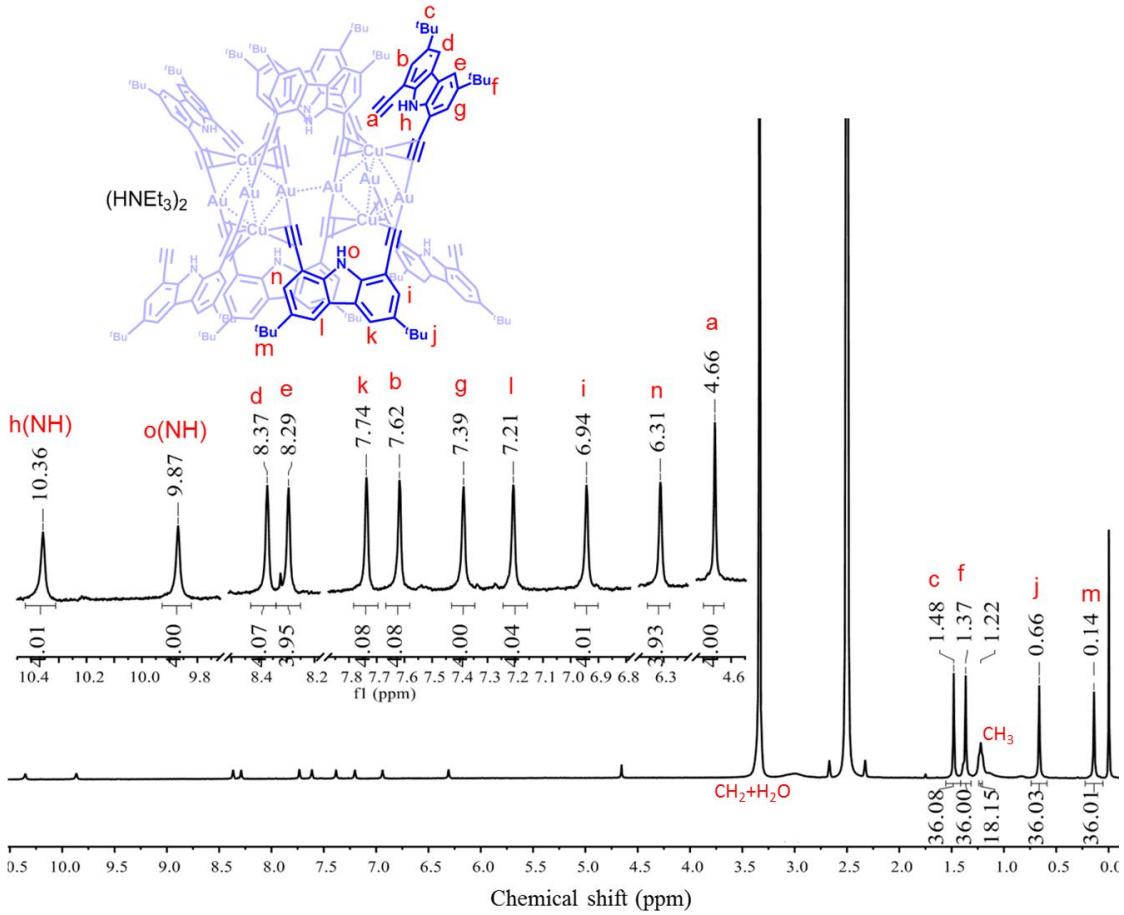

Figure S2. The ^{1}H NMR spectrum of Au_6Cu_4 complex **1** in DMSO-d_6 solution.

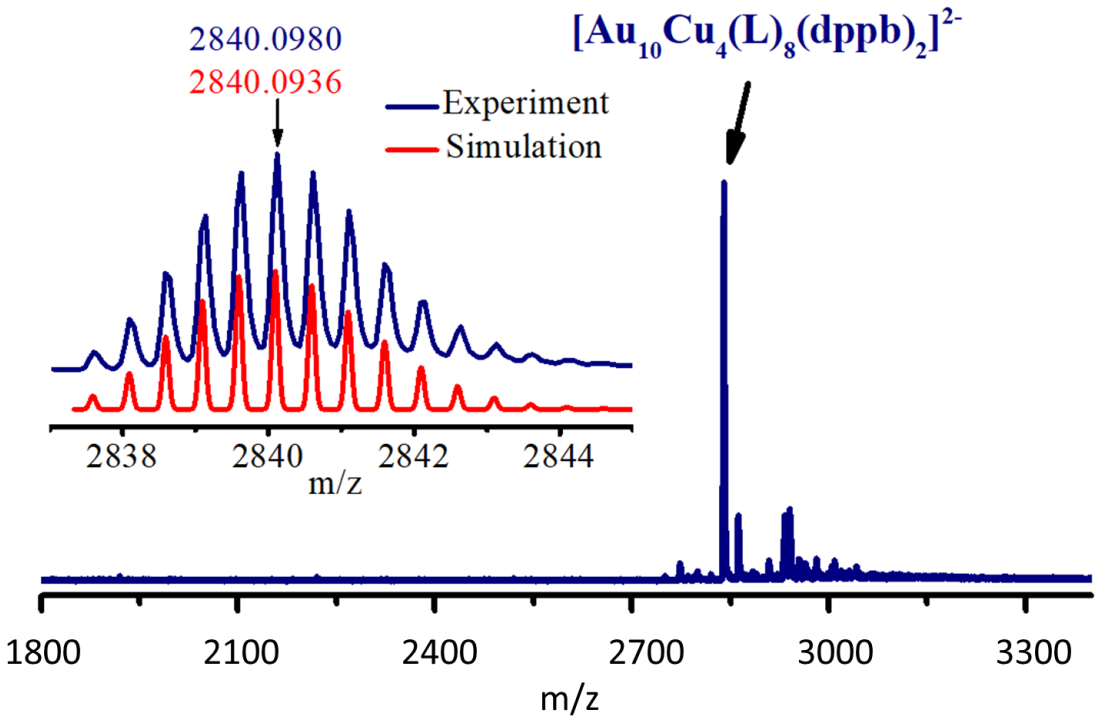

Figure S3. The high-resolution mass spectrometry of $Au_{10}Cu_4$ complex **2**. Inset: the measured (blue) and simulated (red) isotopic patterns.

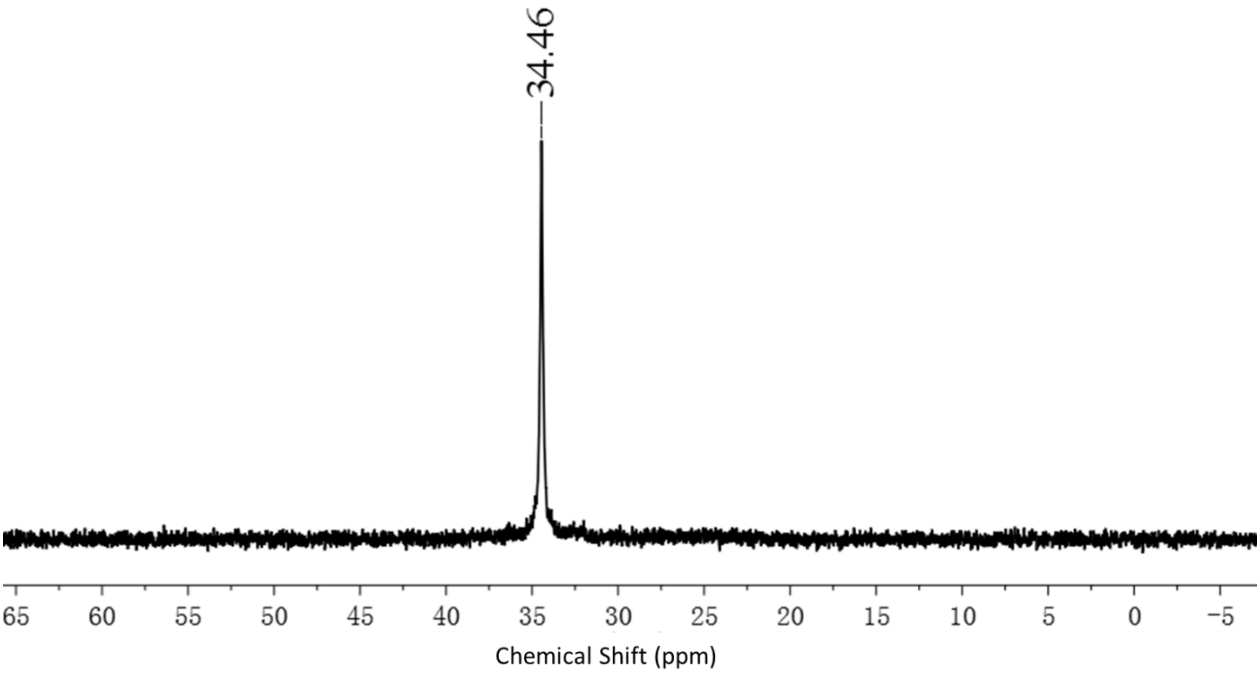

Figure S4. The ^{31}P NMR spectrum of $Au_{10}Cu_4$ complex **2** in CD_2Cl_2 solution.

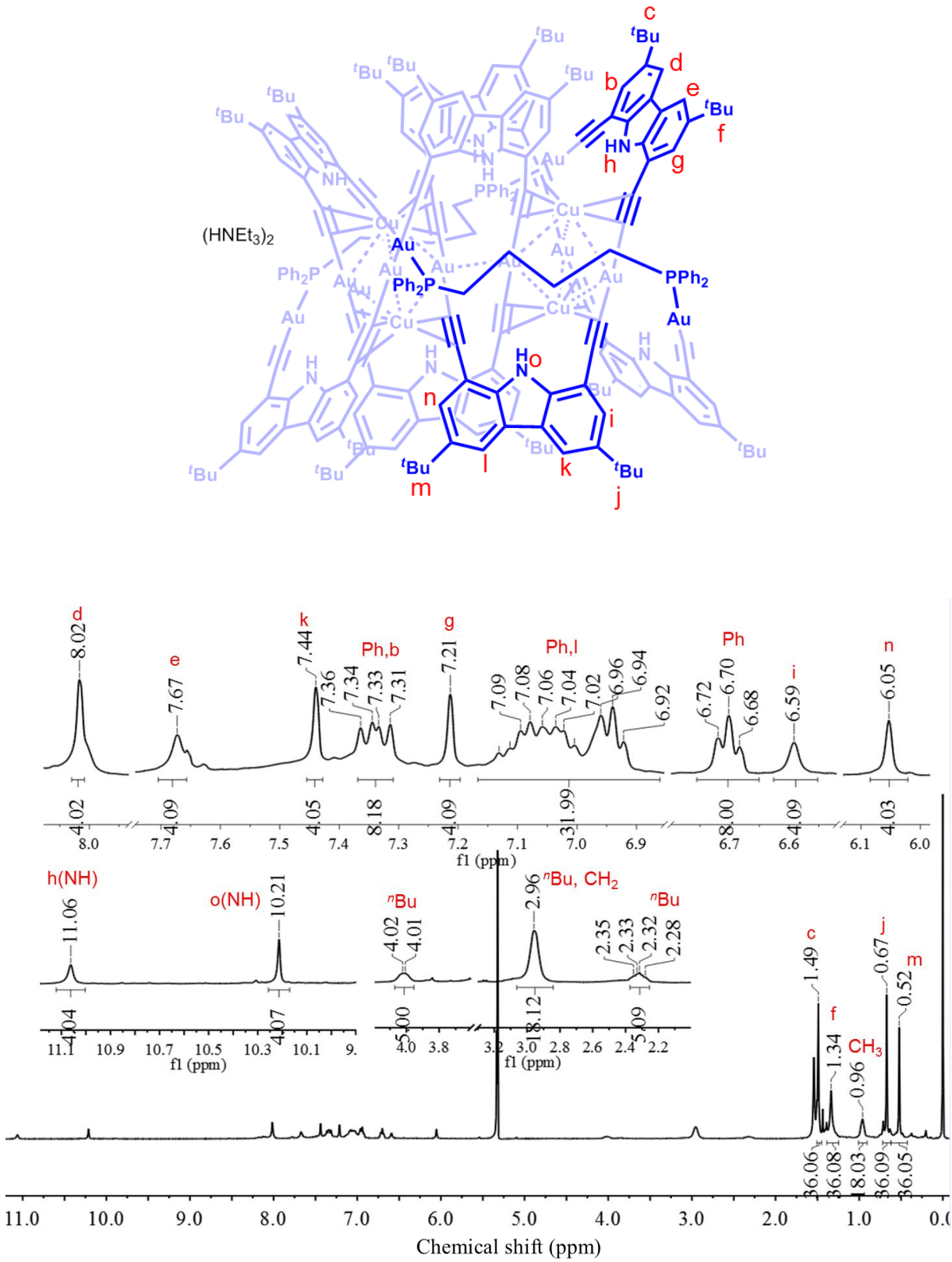

Figure S5. The ^{1}H NMR spectrum of $Au_{10}Cu_4$ complex **2** in CD_2Cl_2 solution.

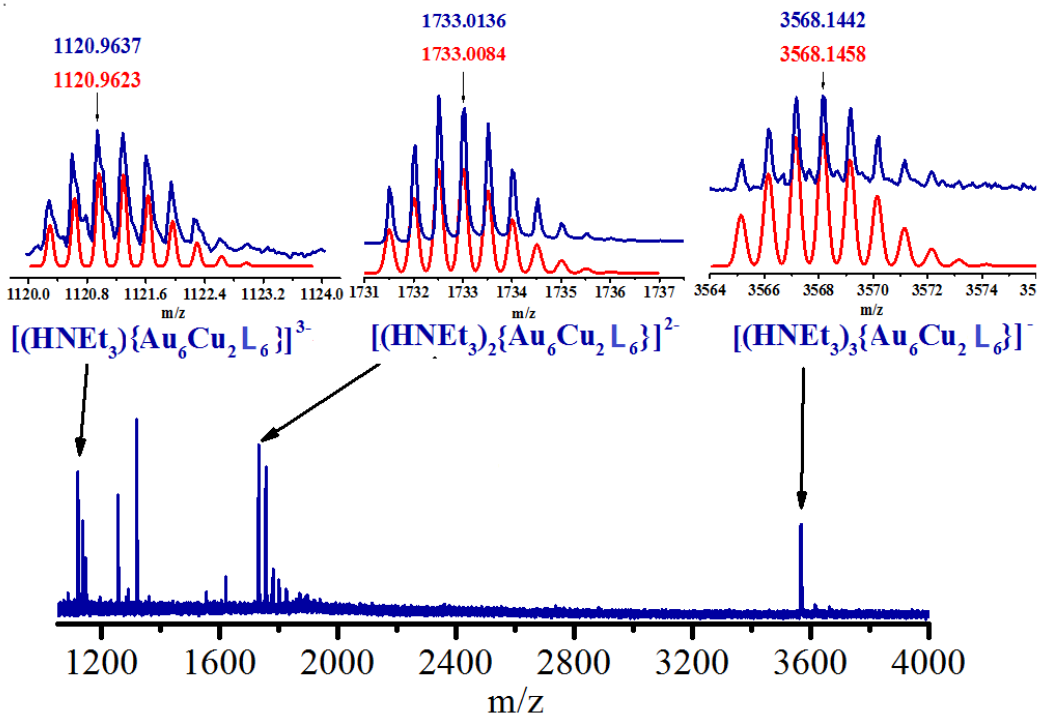

Figure S6. The high-resolution mass spectrometry of Au_6Cu_2 complex **3**. Inset: the measured (blue) and simulated (red) isotopic patterns.

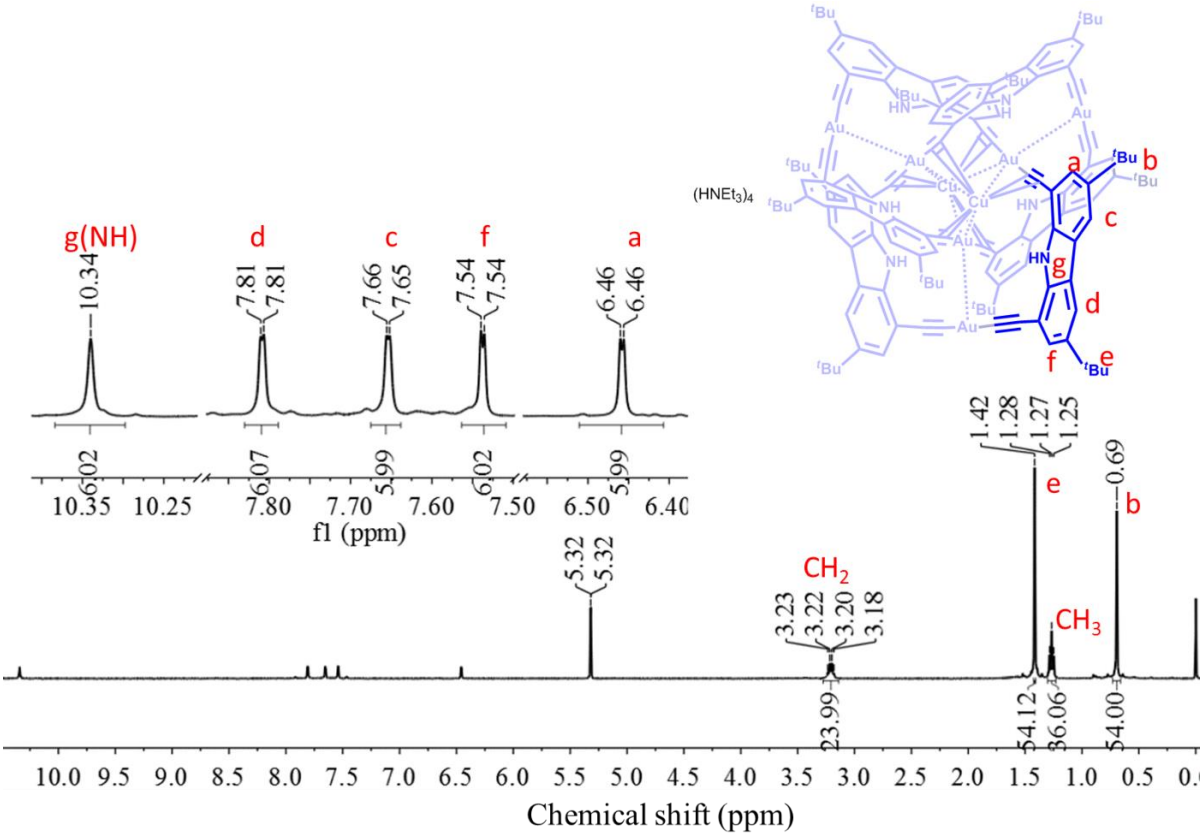

Figure S7. The ^1H NMR spectrum of Au_6Cu_2 complex **3** in CD_2Cl_2 solution.

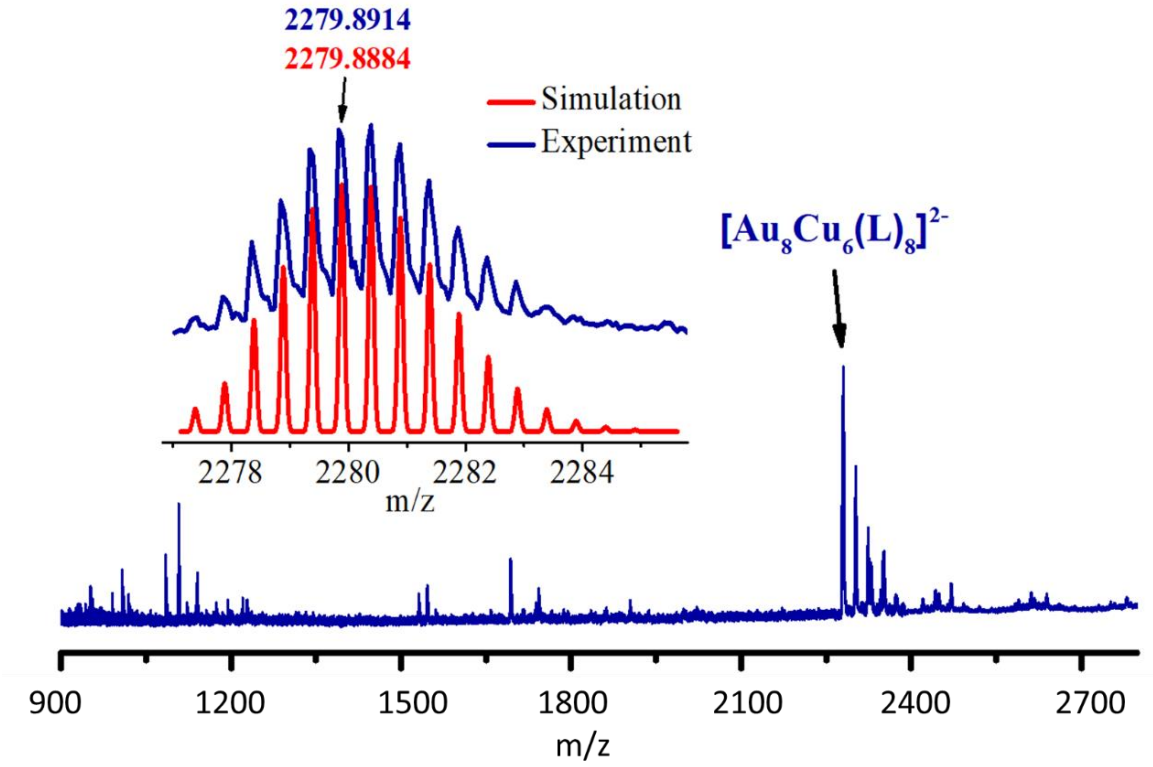

Figure S8. The high-resolution mass spectrometry of Au_8Cu_6 complex **4**. Inset: the measured (blue) and simulated (red) isotopic patterns.

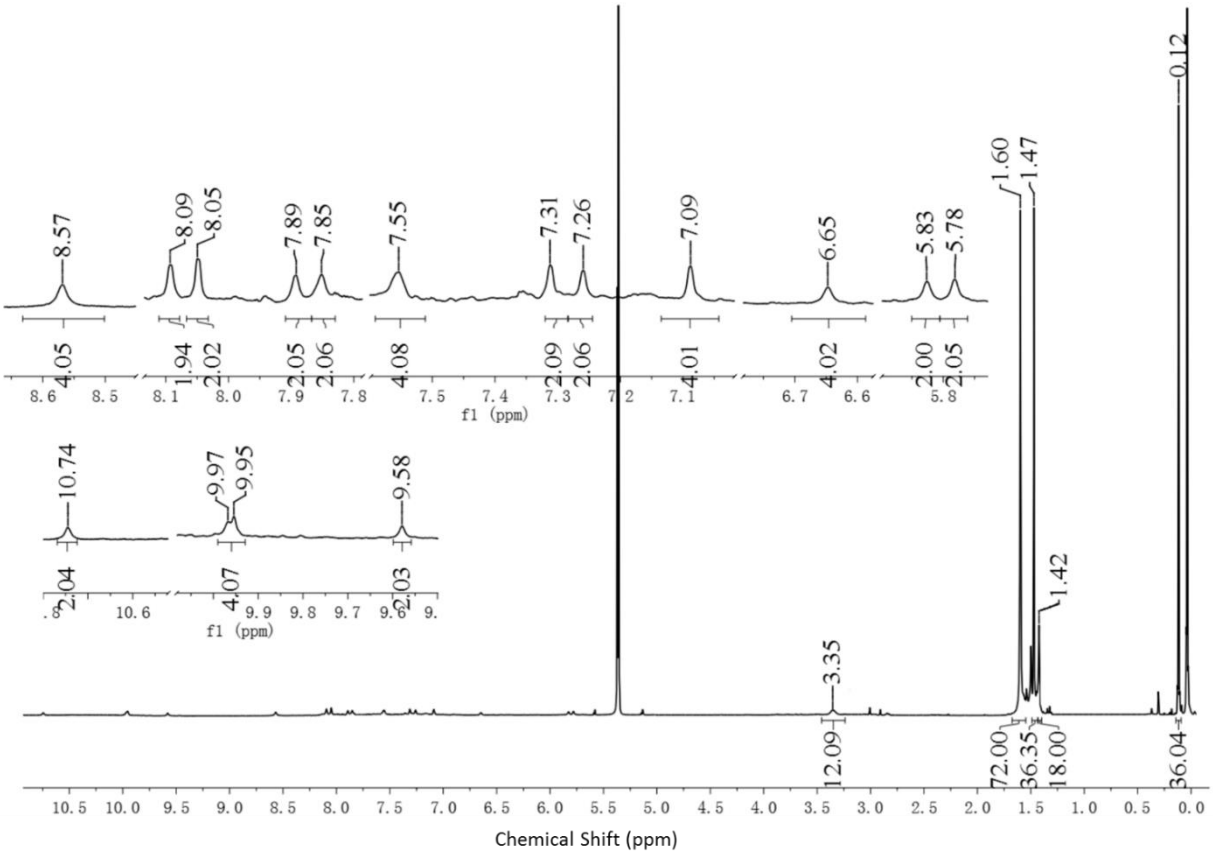

Figure S9. The ^{1}H NMR spectrum of Au_8Cu_6 complex **4** in CD_2Cl_2 solution.

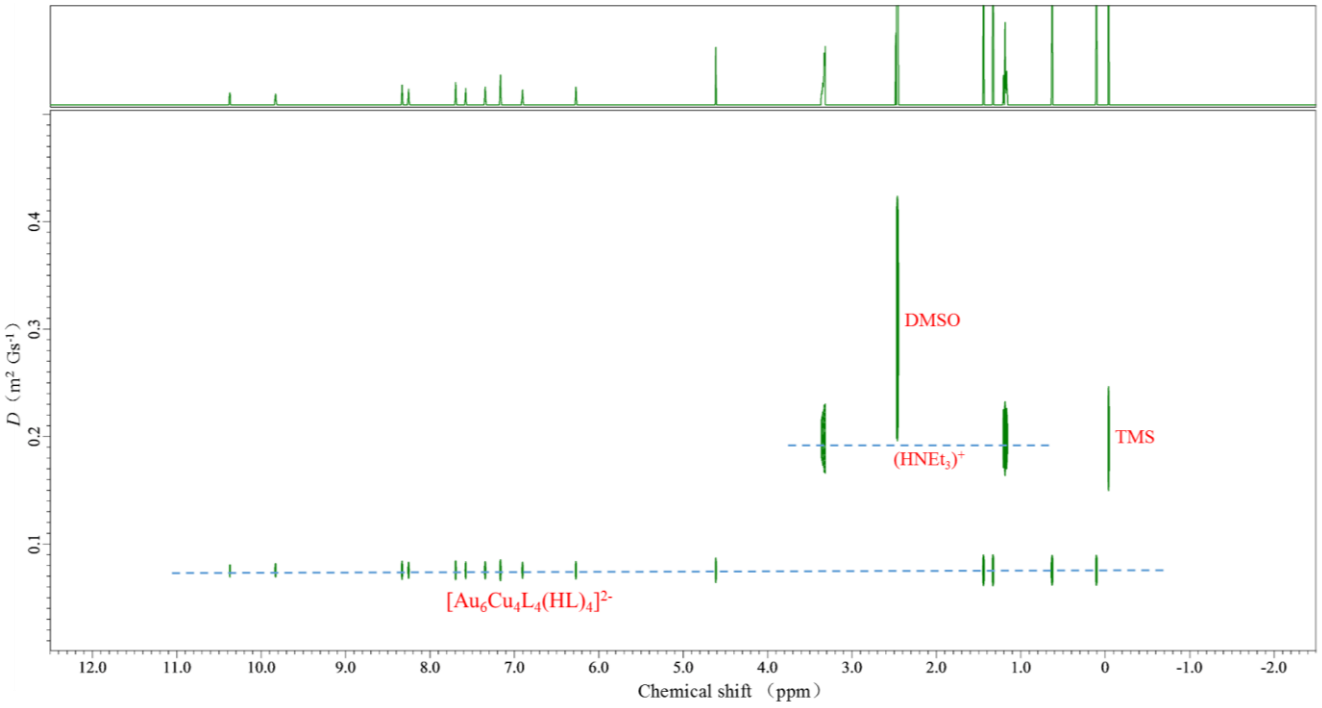

Figure S10. The DOSY NMR spectrum of Au_6Cu_4 complex **1** in DMSO-d_6 solution.

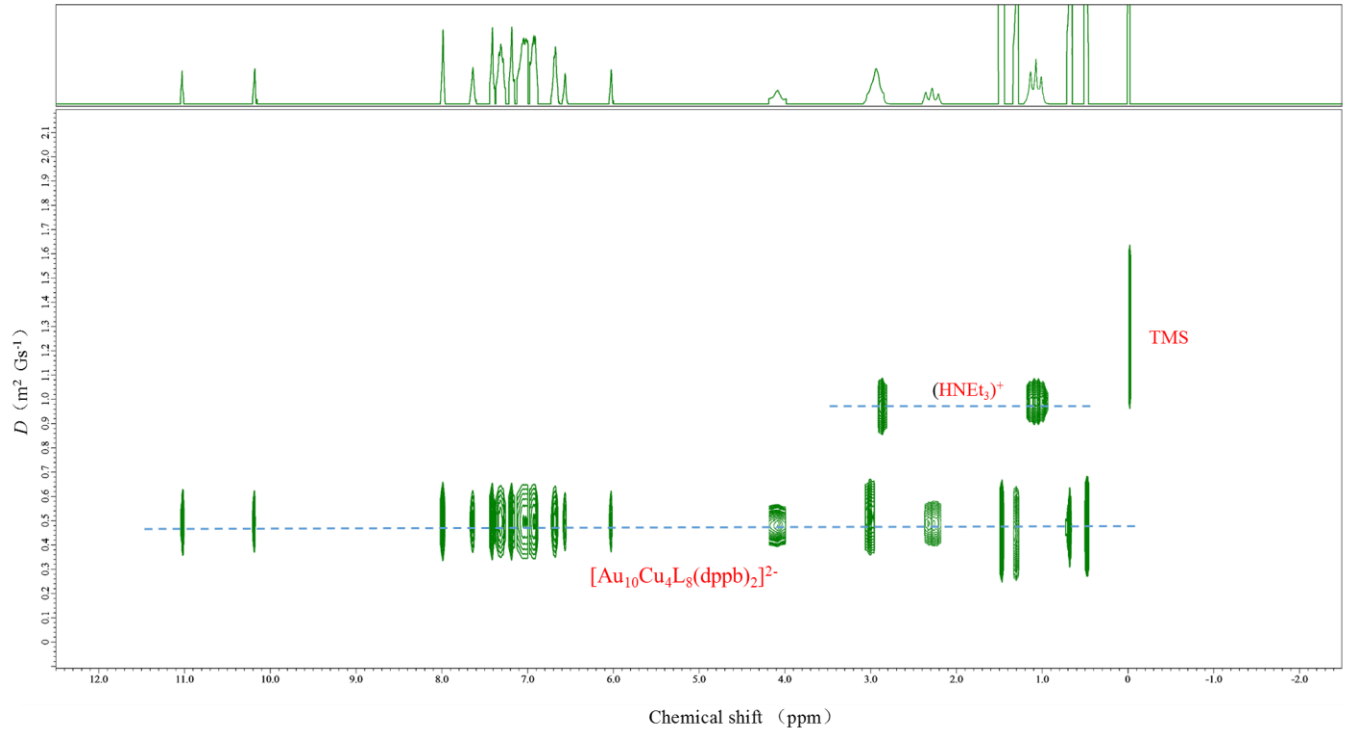

Figure S11. The DOSY NMR spectrum of $Au_{10}Cu_4$ complex **2** in CD_2Cl_2 solution.

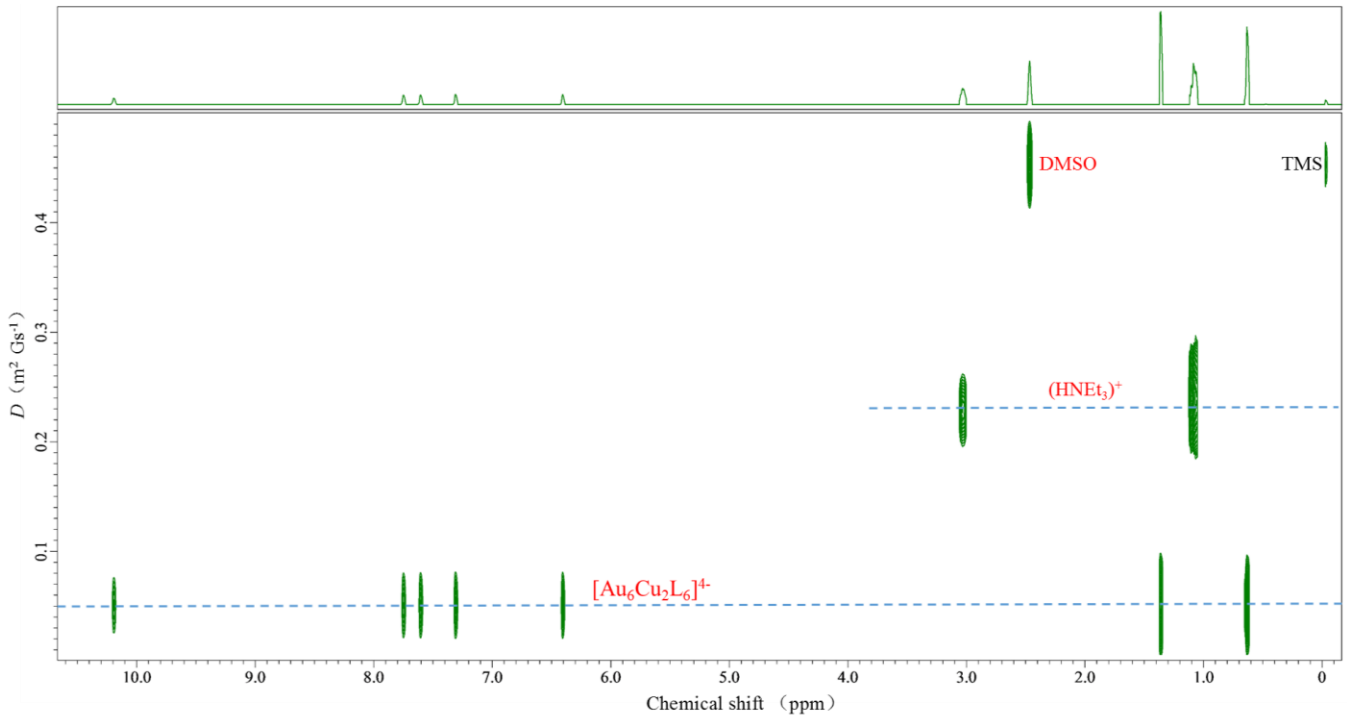

Figure S12. The DOSY NMR spectrum of Au_6Cu_2 complex **3** in DMSO-d_6 solution.

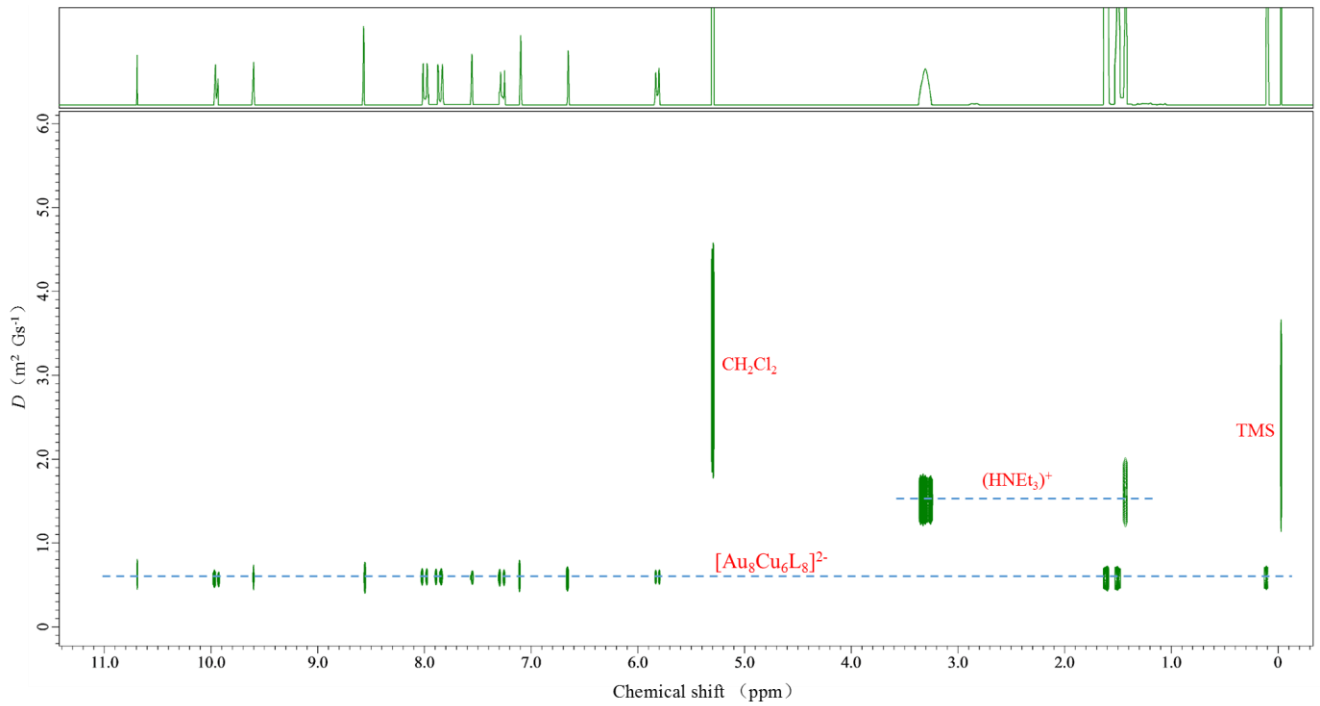

Figure S13. The DOSY NMR spectrum of Au_8Cu_6 complex **4** in CD_2Cl_2 solution.

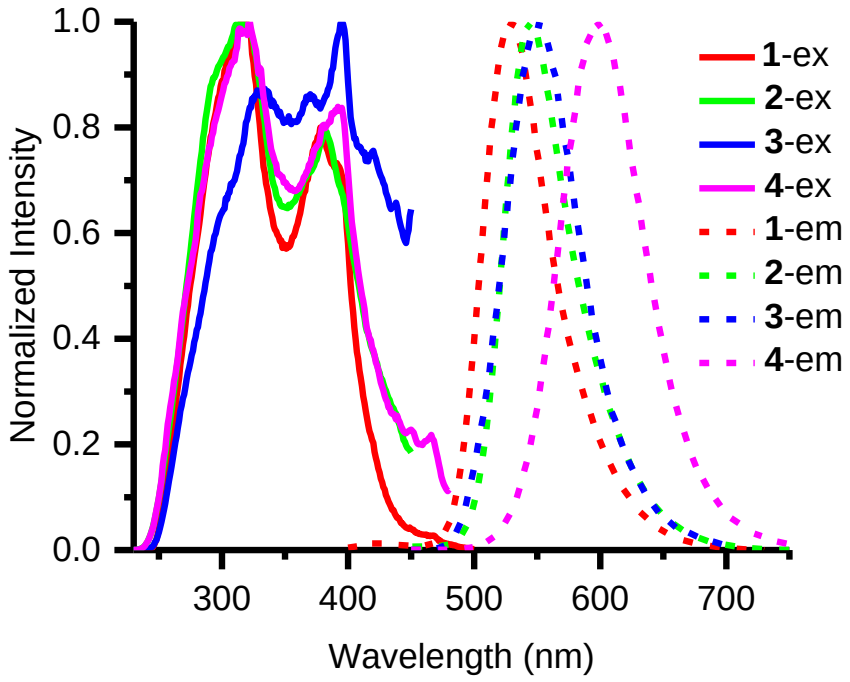

Figure S14. The excitation (solid) and emission (dash) spectra of Au_6Cu_4 complex **1**, $Au_{10}Cu_4$ complex **2**, Au_6Cu_2 complex **3** and Au_8Cu_6 complex **4** in CH_2Cl_2 solutions at ambient condition.

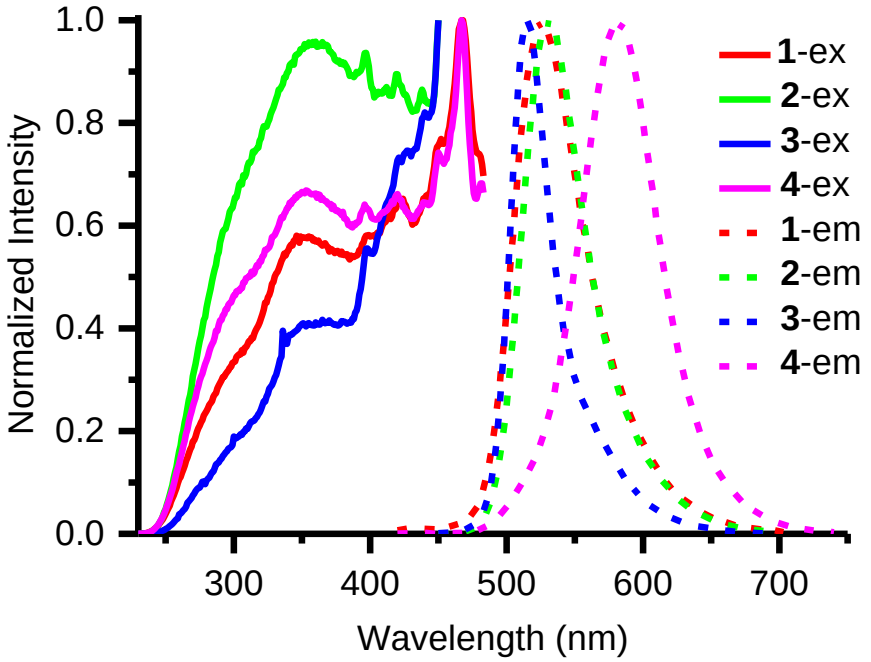

Figure S15. The excitation (solid) and emission (dash) spectra of Au_6Cu_4 complex **1**, $Au_{10}Cu_4$complex **2**, Au_6Cu_2 complex **3** and Au_8Cu_6 complex **4** in solid state at ambient condition.

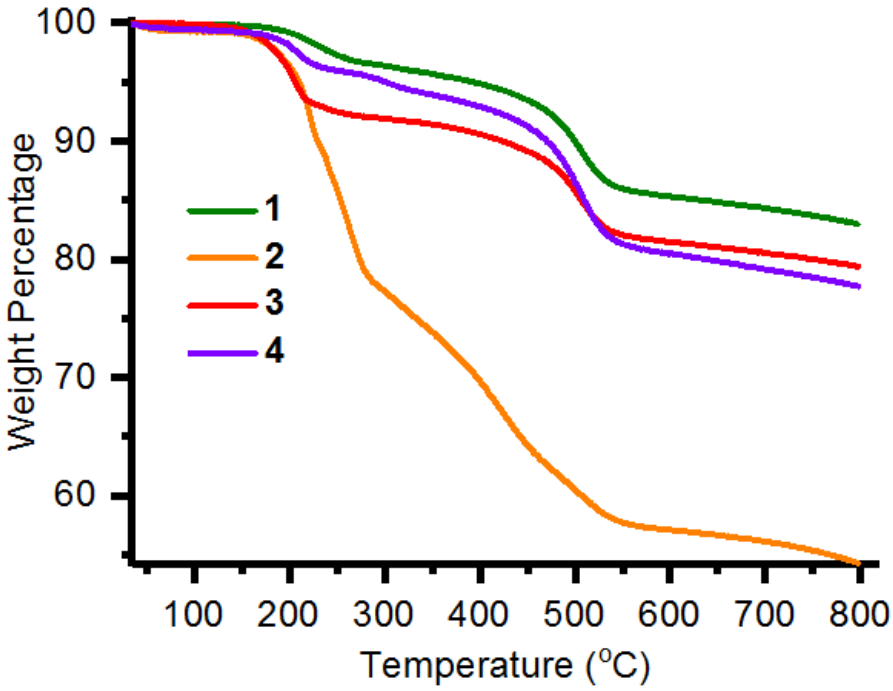

Figure S16. The plots of thermogravimetric analyses of complexes **1**–**4**.

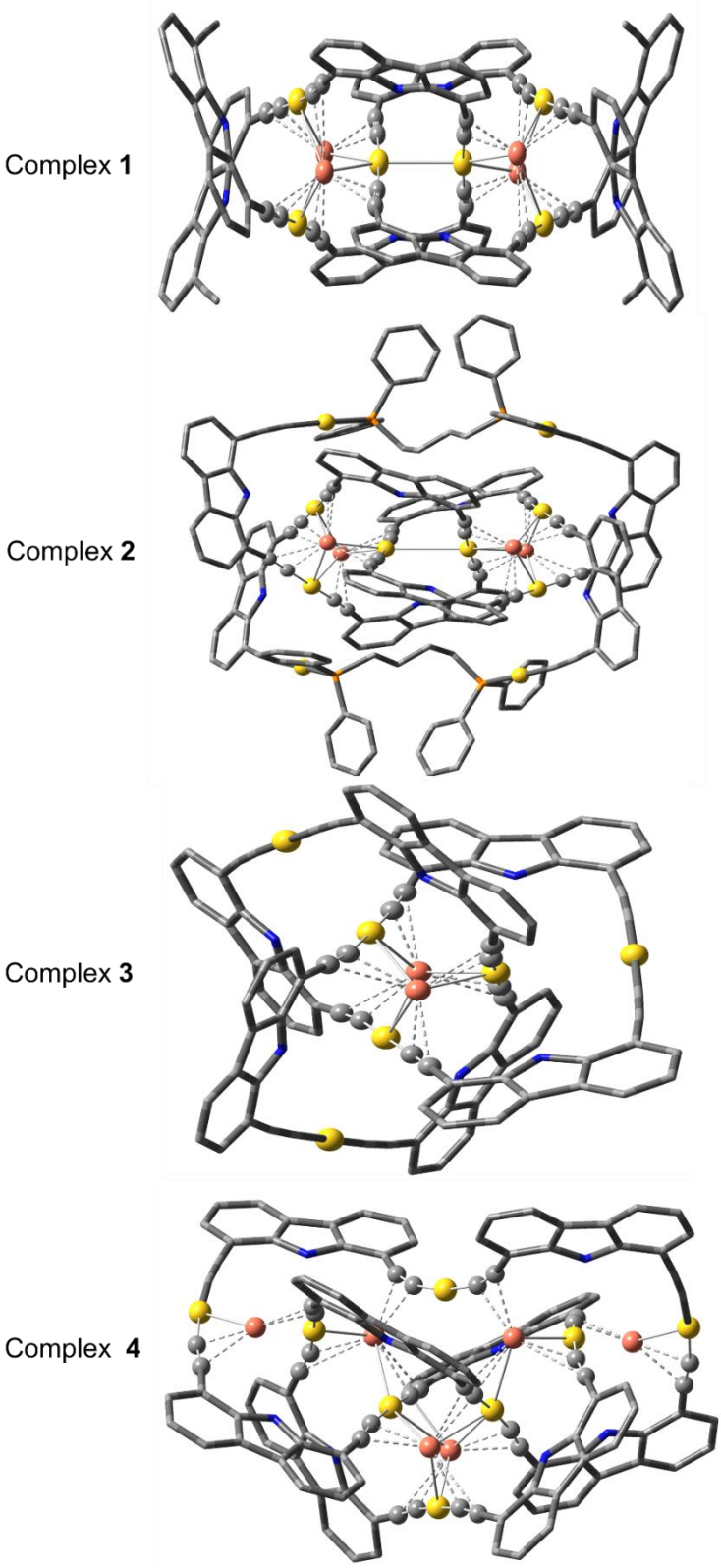

Figure S17. The optimized structures of Au-Cu complexes **1–4** in the ground state (S_0).

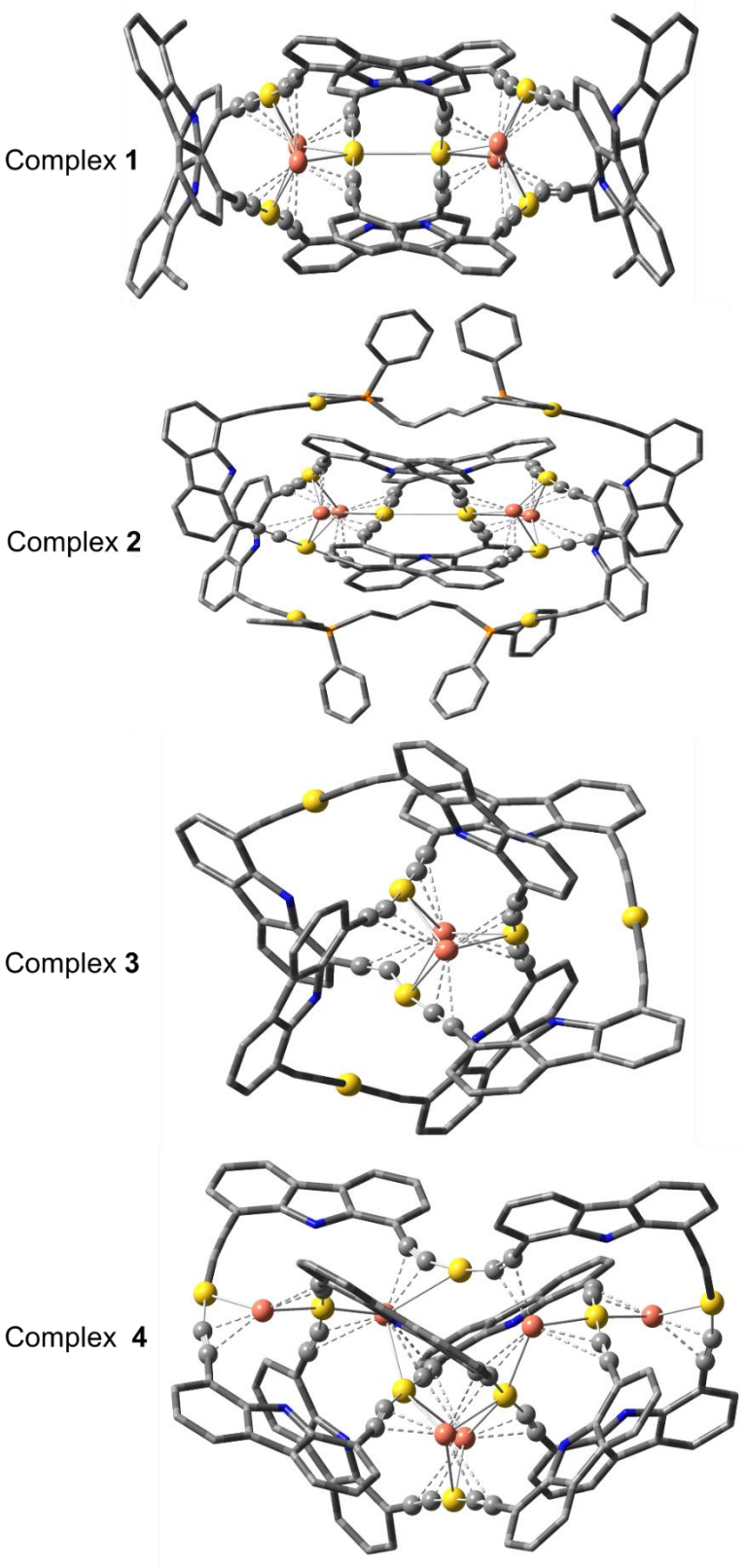

Figure S18. The optimized structures of Au-Cu complexes **1**–**4** in the triplet state (T_1).

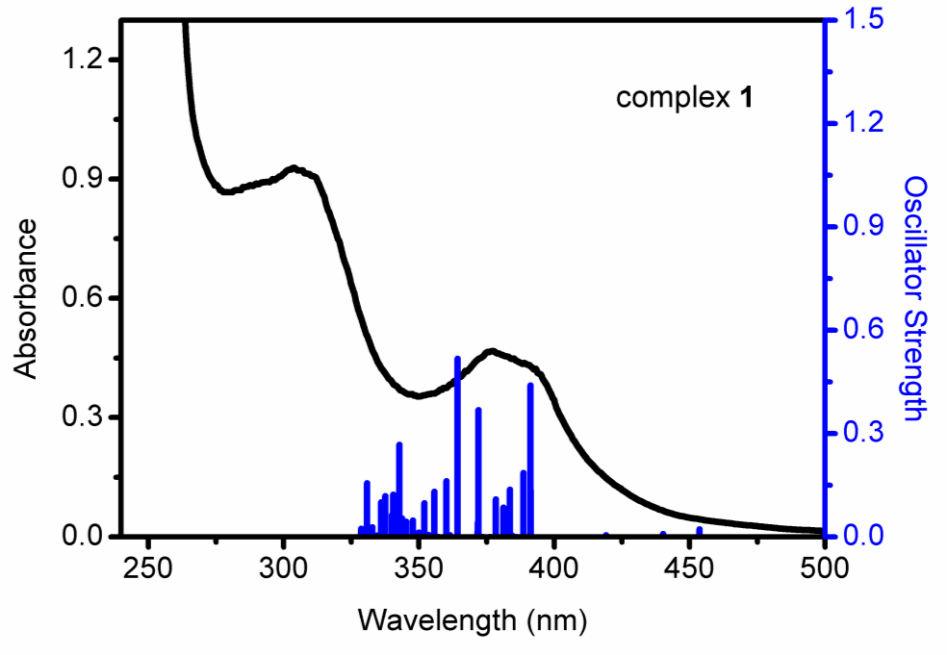

Figure S19. The measured (black line) and calculated (blue bars) absorption spectra of Au_6Cu_4 complex **1** in the CH_2Cl_2 solution at ambient temperature by TD-DFT method at the PBE1PBE level.

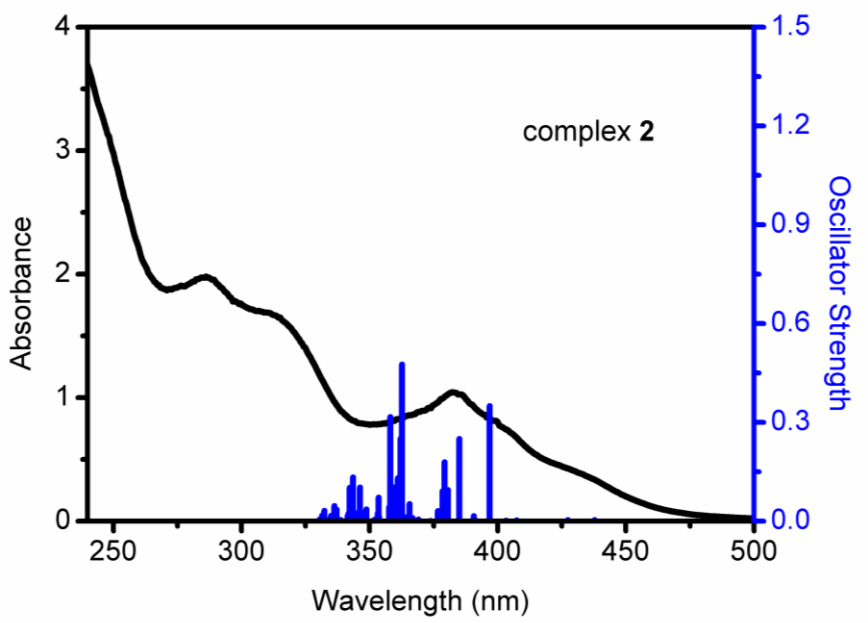

Figure S20. The measured (black line) and calculated (blue bars) absorption spectra of $Au_{10}Cu_4$ complex **2** in the CH_2Cl_2 solution at ambient temperature by TD-DFT method at the PBE1PBE level.

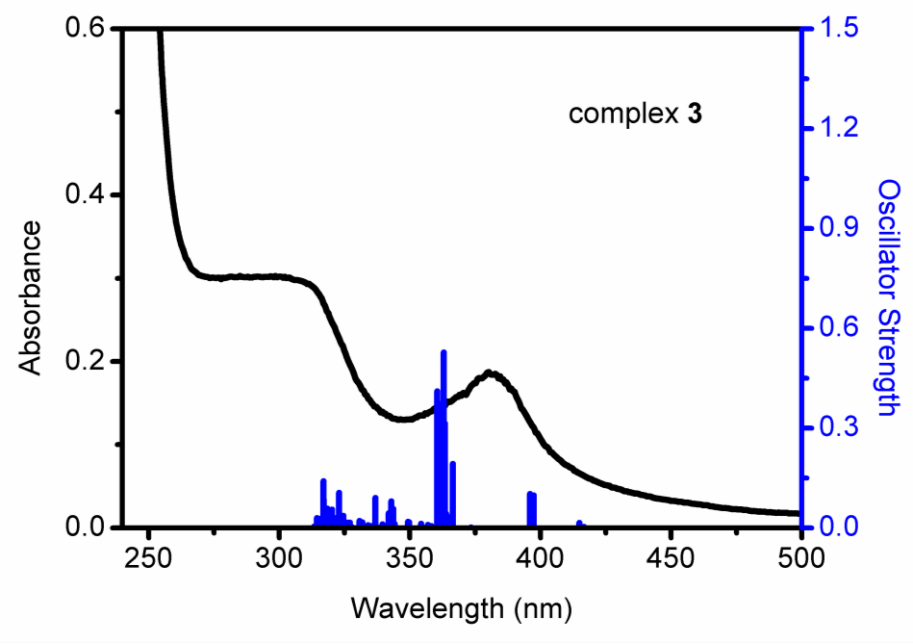

Figure S21. The measured (black line) and calculated (blue bars) absorption spectra of Au_6Cu_2 complex **3** in the CH_2Cl_2 solution at ambient temperature by TD-DFT method at the PBE1PBE level.

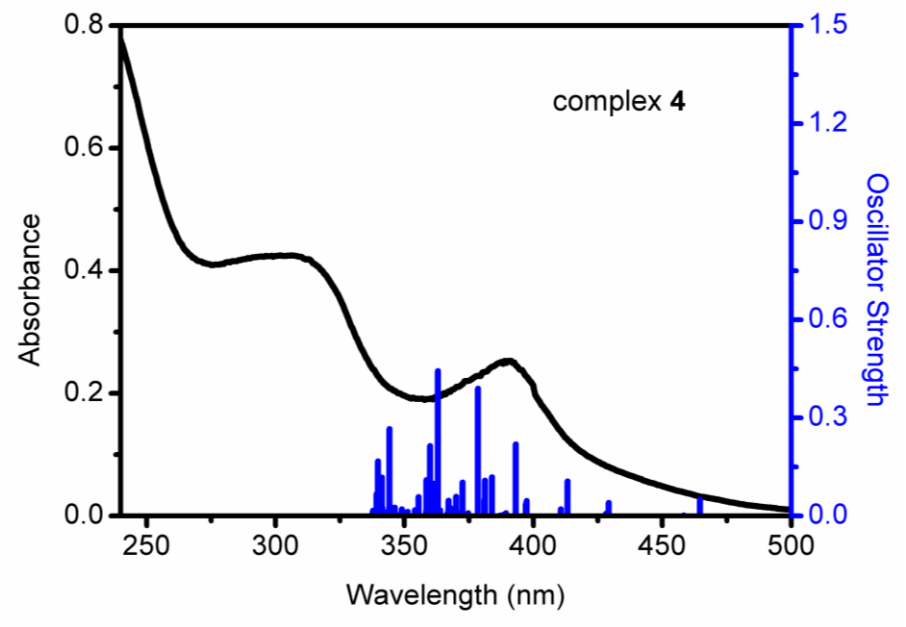

Figure S22. The measured (black line) and calculated (blue bars) absorption spectra of Au_8Cu_6 complex **4** in the CH_2Cl_2 solution at ambient temperature by TD-DFT method at the PBE1PBE level.

complex	HOMO	LUMO
1	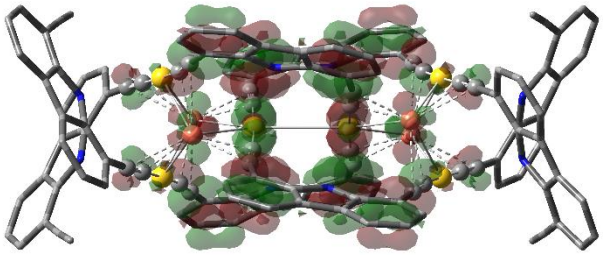	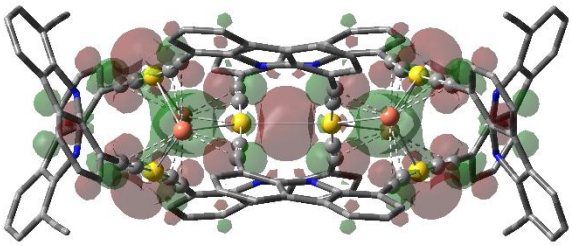
2	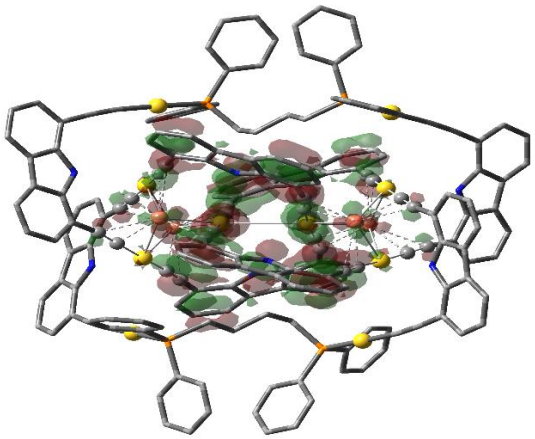	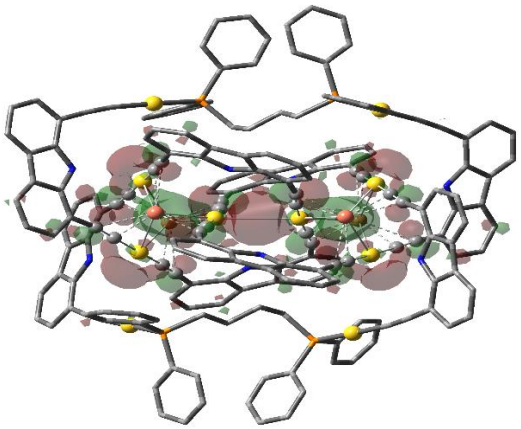
3	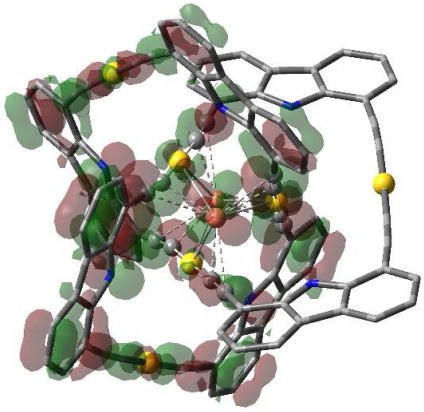	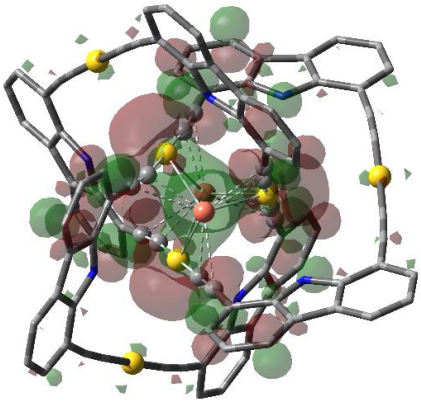
4	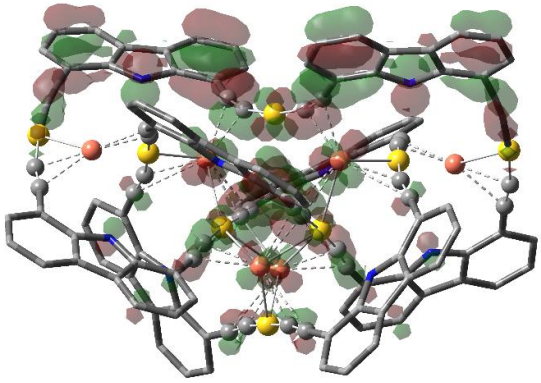	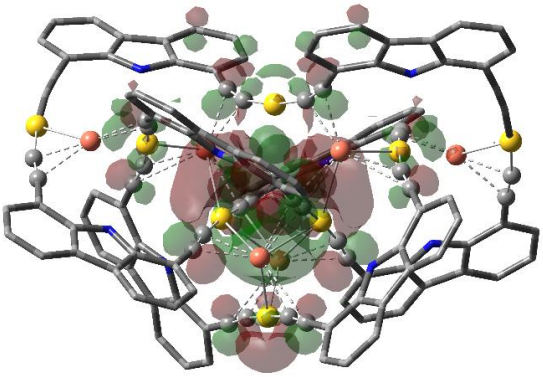

Figure S23. Plots of HOMO and LUMO of Au_6Cu_4 complex **1**, $Au_{10}Cu_4$ complex **2**, Au_6Cu_2 complex **3** and Au_8Cu_6 complex **4** in the ground state (S_0).

REFERENCES

(1) Krause, L.; Herbst-Irmer, R.; Sheldrick, G. M.; Stalke, D., Comparison of silver and molybdenum microfocus X-ray sources for single-crystal structure determination. *J. Appl. Crystallogr.* **2015**, *48*, 3–10.

(2) Hübschle, C. B.; Sheldrick, G. M.; Dittrich, B., ShelXle: a Qt graphical user interface for SHELXL. *J. Appl. Crystallogr.* **2011**, *44*, 1281–1284.

(3) Frisch, M. J.; Trucks, G. W.; Schlegel, H. B.; Scuseria, G. E.; Robb, M. A.; Cheeseman, J. R.; Scalmani, G.; Barone, V.; Petersson, G. A.; Nakatsuji, H.; Li, X.; Caricato, M.; Marenich, A. V.; Bloino, J.; Janesko, B. G.; Gomperts, R.; Mennucci, B.; Hratchian, H. P.; Ortiz, J. V.; Izmaylov, A. F.; Sonnenberg, J. L.; Williams; Ding, F.; Lipparini, F.; Egidi, F.; Goings, J.; Peng, B.; Petrone, A.; Henderson, T.; Ranasinghe, D.; Zakrzewski, V. G.; Gao, J.; Rega, N.; Zheng, G.; Liang, W.; Hada, M.; Ehara, M.; Toyota, K.; Fukuda, R.; Hasegawa, J.; Ishida, M.; Nakajima, T.; Honda, Y.; Kitao, O.; Nakai, H.; Vreven, T.; Throssell, K.; Montgomery Jr., J. A.; Peralta, J. E.; Ogliaro, F.; Bearpark, M. J.; Heyd, J. J.; Brothers, E. N.; Kudin, K. N.; Staroverov, V. N.; Keith, T. A.; Kobayashi, R.; Normand, J.; Raghavachari, K.; Rendell, A. P.; Burant, J. C.; Iyengar, S. S.; Tomasi, J.; Cossi, M.; Millam, J. M.; Klene, M.; Adamo, C.; Cammi, R.; Ochterski, J. W.; Martin, R. L.; Morokuma, K.; Farkas, O.; Foresman, J. B.; Fox, D. J., *Gaussian 16 Rev. C.01*, Wallingford, CT, 2016.

(4) Perdew, J. P.; Burke, K.; Ernzerhof, M., Generalized Gradient Approximation Made Simple. *Phys. Rev. Lett.* **1996**, *77*, 3865–3868.

(5) Bauernschmitt, R.; Ahlrichs, R., Treatment of electronic excitations within the adiabatic approximation of time dependent density functional theory. *Chem. Phys. Lett.* **1996**, *256*, 454–464.

(6) Casida, M. E.; Jamorski, C.; Casida, K. C.; Salahub, D. R., Molecular excitation energies to high-lying bound states from time-dependent density-functional response theory: Characterization and correction of the time-dependent local density approximation ionization threshold. *J. Chem. Phys.* **1998**, *108*, 4439–4449.

(7) Stratmann, R. E.; Scuseria, G. E.; Frisch, M. J., An efficient implementation of time-dependent density-functional theory for the calculation of excitation energies of large molecules. *J. Chem. Phys.* **1998**, *109*, 8218–8224.

(8) Marenich, A. V.; Cramer, C. J.; Truhlar, D. G., Universal solvation model based on solute electron density and a continuum model of the solvent defined by the bulk dielectric constant and atomic surface tensions. *J. Phys. Chem. B* **2009**, *113*, 6378-6396.

(9) Andrae, D.; Häussermann, U.; Dolg, M.; Stoll, H.; Preuss, H., Energy-adjusted ab initio pseudopotentials for the second and third row transition elements. *Theor. Chim. Acta.* **1990**, *77*, 123–141.

(10) Ros, P.; Schuit, G. C. A., Molecular Orbital Calculations on Copper Chloride Complexes. *Theo. Chim. Acta (Berl.)* **1966**, *4*, 1–12.

(11) Lu, T.; Chen, F.-W., Multiwfn: A Multifunctional Wavefunction Analyzer. *J. Comp. Chem.* **2012**, *33*, 580–592.